Journal of Alloys and Compounds 597 (2014) 155–160

Contents lists available at ScienceDirect

Journal of Alloys and Compounds

journal homepage: www.elsevier.com/locate/jalcom

High-pressure structural phase transitions and intermediate phases of magnesium fluoride

Hülya Öztürk *, Cemile Kürkçü, Cihan Kürkçü

Fizik Bölümü, Ahi Evran Üniversitesi, Kırşehir 40100, Turkey

ARTICLE INFO

Article history:
Received 25 October 2013
Received in revised form 27 January 2014
Accepted 28 January 2014
Available online 5 February 2014

Keywords:
Structural phase transformation
Ab initio molecular dynamics
Intermediate phase

ABSTRACT

We investigate the structural behavior of magnesium fluoride (MgF_2) under the hydrostatic pressure using constant pressure ab initio technique up to 130 GPa. Through constant pressure simulations, two high-pressure phases of MgF_2 are estimated. MgF_2 undergoes a phase transformation from the rutile-type structure to the $CaCl_2$-type structure with space group *Pnnm* at 10–20 GPa. Another phase transformation from the $CaCl_2$-type structure to the α-$PbCl_2$-type structure with space group *Pnma* occurs at 80–90 GPa. The later transformation is based on three intermediate phases with space groups $P2_1/m$, $P2_1$ and $P2_12_12_1$. These phase transitions are also analyzed from the total energy and enthalpy calculations. These phase changes should occur around 9 and 35 GPa from enthalpy calculations, respectively.

1. Introduction

Magnesium fluoride is an important material which takes attention thanks to its wide range of applications. This material is expected to have technological properties hence a number of studies on it have been carried out [1–15]. The magnesium fluoride crystallizes in a tetragonal rutile-type structure with space group $P4_2/mnm$ at ambient conditions which is isomorphic to those TiO_2 (rutile) and SiO_2 (stishovite). Transition metal compounds of BF_2-type such as MnF_2, FeF_2, NiF_2, CoF_2 and ZnF_2 all have the same rutile structure with space group $P4_2/mnm$. Although MgF_2 crystal has also the same rutile structure as the transition metal compounds of BF_2-type, Mg is not a transition metal; namely, Mg has no d-electrons. Deficiency of these electrons and the highly ionic character of magnesium fluoride simplify the theoretical studies. The phase transitions of MgF_2 are obtained at lower pressures than in many dioxides due to the higher compressibility of this substance and relative sizes of its ions. These transitions can be studied under hydrostatic or nearly hydrostatic conditions.

The high-pressure behavior of MgF_2 is quite interesting. Although some studies cited above emphasize that the tetragonal rutile-type MgF_2 should be transformed into a cubic fluorite-type structure with space group $Fm\bar{3}m$, some other studies indicate that the structure should be transformed into an orthorhombic $CaCl_2$-type structure with space group *Pnnm* at high pressures [10,11]. The results of this study show that no fluorite-type phase is present for MgF_2 at high pressure. For this material, the results of our calculations yield the following sequence of the stable phases: rutile → $CaCl_2$ → α-$PbCl_2$, with an overall increase in the coordination number of Mg from 6 to 9.

Haines et al. [9] have studied on both experimental and theoretical methods, e.g., angle-dispersive x-ray powder diffraction and the investigation of the phase stability and structural parameters using density-functional theory. They have observed a phase transition from the tetragonal rutile-type to an orthorhombic $CaCl_2$-type structure at 9.1 GPa prior to the transformation at close to 14 GPa to the cubic phase, which is found to have a modified fluorite structure of the PdF_2-type. A denser cotunnite-type (α-$PbCl_2$) phase is observed at pressures above 35 GPa [9,10]. Wevers et al. [16,17] have investigated the energy landscapes of alkalineearth (e.g. Mg and Ca) fluorides and chlorides and predicted the existence of many metastable modifications. A metastable compound that corresponds to a locally ergodic region of the energy landscape and to the local minima suggests new possible structure types in BX_2 systems. The rate of transition between two local minima and their equilibration are controlled by the energetic barriers. Mu et al. [18] showed that the $CaCl_2$-modification can be stabilized as a metastable nanocrystalline phase at standard pressure. Further recent study by Hoffmann and Schon [19] deals with the optimization of temperature driven phase changes in MgF_2.

Curious structural features of transition mechanism are still unknown owing to difficulties in monitoring movements of atoms during the experiments. In the present work, we offer a simulation study of the transformation mechanism of MgF_2. We suggest the orthorhombic α-$PbCl_2$-type structure of this substance with space

* Corresponding author. Tel.: +90 386 2804555; fax: +90 386 2804525.
E-mail addresses: hozturk@ahievran.edu.tr, hulyaozturk@gazi.edu.tr (H. Öztürk).

http://dx.doi.org/10.1016/j.jallcom.2014.01.221
0925-8388/

group *Pnma* is based on three intermediate phases with space groups $P2_1/m$, $P2_1$ and $P2_12_12_1$, expressed as MgF_2-(1), MgF_2-(2) and MgF_2-(3), respectively. As far as we know, these intermediate states obtained in our study have not been observed in any earlier studies.

2. Computational method

The computations were performed via the ab initio program SIESTA based on pseudopotentials and a localized basis set [20]. Calculations were carried out through the density functional theory (DFT). To find out the exchange-correlation energy, we performed the generalized gradient approximation (GGA) [21]. It has been found that generally double-ξ singly polarized (DZP) bases give precisions within the accuracy of GGA functionals for geometries, energetics and elastic/vibrational properties by Artacho et al. [22]. To calculate the potential energy, a combined Coulomb and Lennard-Jones potential is applied for ionic crystals. The van der Waals r^{-6} term expresses the attraction due to the polarization of the ions while the r^{-12} term in the Lennard-Jones part controls the repulsion between neighboring ions.

In order to describe valence electrons and norm-conserving nonlocal pseudopotentials of atomic core, we considered a localized linear combination of atomic orbital basis sets. For the pseudopotential approximation, plane wave basis sets are always used practically. The plane wave pseudopotential method is simple and very efficient in exploring structural phase transitions. We establish norm-conservative pseudopotentials using Troullier–Martins schemes [23].

In order to represent the electron density, the local part of the pseudopotentials, the Hartree and the exchange-correlation potential, we used a uniform mesh with a plane wave cut-off of 150 Ry. We have chosen the simulation cell of 96 atoms and used periodic boundary conditions. We employed double-ξ plus polarized basis sets and used Γ-point sampling for the Brillouin zone integration. The Brillouin zone integration was carried out with an automatically generated 6–6–6 *k*-point mesh for the phases prepared according to the method of Monkhorst and Pack [24]. The plane-wave cut-off and *k*-point sampling are sufficient for full convergence. The structures were allowed to relax and to find their equilibrium volumes and lowest energies for each value of the applied pressure by optimizing their lattice vectors and atomic positions together until the maximum atomic forces were getting smaller until 0.01 eV $Å^{-1}$ and the stress tolerances were getting less until 0.5 GPa. It was used a variable-cell shape conjugate-gradient method under a constant pressure for minimization of geometries.

In order to apply pressure to the system, we used the Parrinello and Rahman method [25]. Initially the system was relaxed at zero pressure, afterwards pressure was gradually increased. The structure was equilibrated at each applied pressure through 1 ps. We have started from the beginning at each pressure step from the equilibrated coordinates of previous steps in order to make sure the pressure path to be continuous. In order to identify symmetries of the phases observed in the simulations, we used the RGS algorithm and the KPLOT program [26,27] that allow detailed information about a given structure such as space group, cell parameters and atomic positions. For the energy–volume calculations, we used the unit cells for the rutil-type, $CaCl_2$-type and α-$PbCl_2$-type structures.

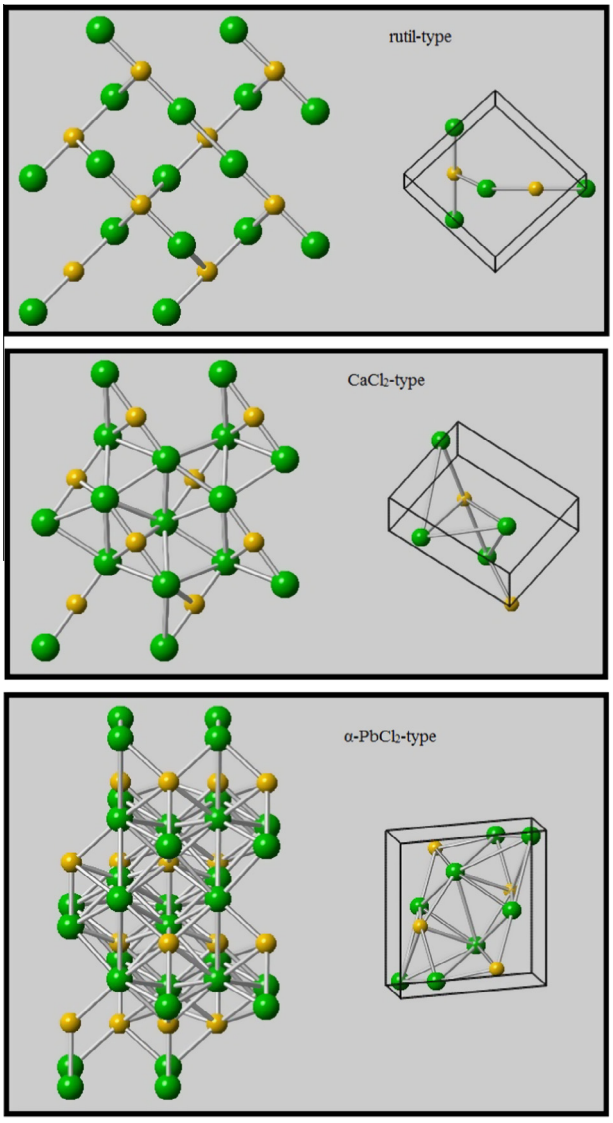

Fig. 1. Crystal structures with unit cells of MgF_2: rutile-type structure at zero pressure (as illustrated in the first panel), $CaCl_2$-type structure at 20 GPa (in the second panel) and α-$PbCl_2$-type structure at 90 GPa (in the third panel). All structures are viewed along *z*-direction and the unit cells are viewed along N(1 1 1) directions.

3. Results

Pressure was gradually increased beginning from the zero-pressure structure and the structure of MgF_2 at each applied pressure was analyzed via the KPLOT program. A phase transformation into the orthorhombic $CaCl_2$-type structure with a space group *Pnnm* has been found at 20 GPa. It has 6 atoms per unit cell. The softening of the elastic shear module (C_s) in the rutile phase and the decrease of the square of the spontaneous strain (e_{ss}) from the $CaCl_2$-type structure supported this result [28]. At 90 GPa we have found another phase transformation into the α-$PbCl_2$-type structure with space group *Pnma*. It has 12 atoms per unit cell. These structures are depicted in Fig. 1 with unit cells.

Mg is six-, six- and nine-fold coordinated by F for the rutile-type structure, the $CaCl_2$-type structure and the α-$PbCl_2$-type structure, respectively. The Mg–F bond lengths range from 1.981 to 1.996 Å and the F–F bond lengths are 2.549 Å for the rutile-type structure. The Mg–F bond lengths range from 1.892 to 1.924 Å and the F–F bond lengths range from 2.460 to 2.709 Å for the $CaCl_2$-type structure. The Mg–F bond lengths range from 1.845 to 2.206 Å and the F–F bond lengths range from 2.185 to 2.579 Å for α-$PbCl_2$-type structure.

In order to elucidate the mechanism of these phase transitions, pressure dependence of the simulation cell vectors and angles should be examined. These cell vectors expressed as **A**, **B**, and **C** are initially along the [100], [010] and [001] directions, correspondingly. Fig. 2 depicts variation of the simulation cell lengths and angles as a function of minimization step at 20 and 90 GPa, respectively.

In order to investigate whether there is any intermediate state during the phase transformations or not, we analyzed the structure obtained in that study at each minimization step via the KPLOT program. We determine a monoclinic structure expressed as MgF_2-(1) having $P2_1/m$ symmetry at 412 minimization step, another monoclinic structure expressed as MgF_2-(2) having $P2_1$ symmetry at 517 step and also an orthorhombic structure expressed as MgF_2-(3) having $P2_12_12_1$ symmetry at 553 step. These intermediary structures corresponding to local minima are depicted in Fig. 3. The orthorhombic α-$PbCl_2$-type structure having *Pnma* symmetry forms at 580 minimization step. The Mg is six-, nine- and nine-fold coordinated by F for MgF_2-(1), MgF_2-(2) and MgF_2-(3), respectively.

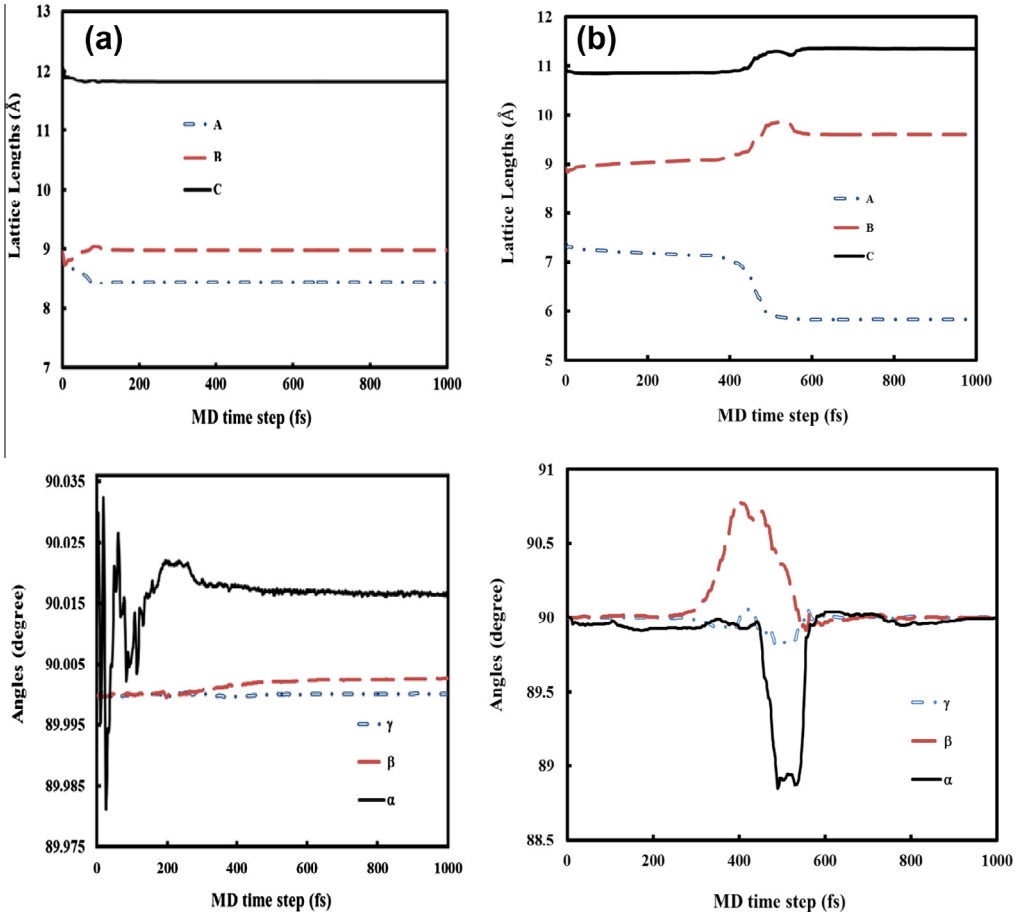

Fig. 2. The time evolution of the simulation cell lengths (A marked with "", B with "", C with "") and angles (γ marked with "", β with "", α with "") at 20 GPa depicted in (a), at 90 GPa depicted in (b). (For interpretation of the references to colour in this figure legend, the reader is referred to the web version of this article.)

The F is three-, four- and five-fold coordinated by Mg for MgF_2-(1), MgF_2-(2) and MgF_2-(3), respectively. The Mg–F bond lengths range from 1.771 to 1.819 Å and the F–F bond lengths range from 2.181 to 2.737 Å for MgF_2-(1). The Mg–F bond lengths range from 1.760 to 2.347 Å and the F–F bond lengths range from 2.095 to 2.660 Å for MgF_2-(2). The Mg–F bond lengths range from 1.805 to 2.272 Å and the F–F bond lengths range from 2.128 to 2.736 Å for MgF_2-(3).

We have drawn the pressure–volume dependence depicted in Fig. 4 in order to identify the thermodynamic nature of the phase transitions in MgF_2. As seen in this figure, the volume decreases monotonically and shows small discontinuities at 20 GPa and 90 GPa. These discontinuities indicate the phase transitions. As expected, the structure transforms to the orthorhombic $CaCl_2$-type structure with space group *Pnnm* at 20 GPa and the orthorhombic $CaCl_2$-type structure transforms to the orthorhombic α-$PbCl_2$-type structure with space group *Pnma* at 90 GPa. These structures are shown in Fig. 1 and its parameters are summarized in Table 1. In order to examine whether there are another phase transformations or not, we have increased the pressure up to 130 GPa.

Since transition pressures obtained in constant-pressure simulations are generally overestimated, we take the energy–volume computations into account so as to study the stability of high-pressures phases of MgF_2. For these calculations, we considered the unit cell for MgF_2 phases. The calculated total energy–volume dependences are fitted to the third-order Birch–Murnaghan equation of states given by

$$P = 1.5B_0\left[(V/V_0)^{-7/3} - (V/V_0)^{-5/3}\right]x\left\{1 + 0.75(B_0' - 4)\left[(V/V_0)^{-2/3} - 1\right]\right\}$$

where P is the applied pressure, V is the volume at pressure, V_0, B_0 and B_0' are the volume, bulk modulus and its pressure derivative at ambient pressure [29,30]. Fig. 5 shows the total energy as a function of volume. We have presented the equilibrium lattice parameters, equilibrium volume rates, bulk modules and their pressure derivatives with available experimental and theoretical results in Table 2. Although our equilibrium lattice parameters and equilibrium volumes have a real physical meaning, B_0 and B_0' are the fit parameters from Murnaghan formula.

The phonon contributions and the Gibbs free energies are also important [31,32]. We can easily identify the relative stability of the different phases of MgF_2 under finite pressure and temperature by a simple compression of their Gibbs free energies, $G = E_{tot} + PV - TS$. The TS term is neglected because calculations are made at zero temperature. Thus, the static enthalpy can be expressed as $H = E_{tot} + PV$, where pressure is obtained by direct differentiation of the energy–volume curves *i.e.*, $P = -dE_{tot}/dV$ [33]. Since structural phase transformations in simulations occur across the entire simulation cells, systems have to cross a significant energy barrier to transform from one phase to another one. Enthalpy calculations give often reasonable transition pressures relative to experiments. For that reason, we calculate the enthalpy of the phases. The phase transitions occur when the enthalpies of the two phases equal to each other, that is, we use the thermodynamic criterion of equal free energies in order to predict accurate critical pressure. Fig. 6 shows

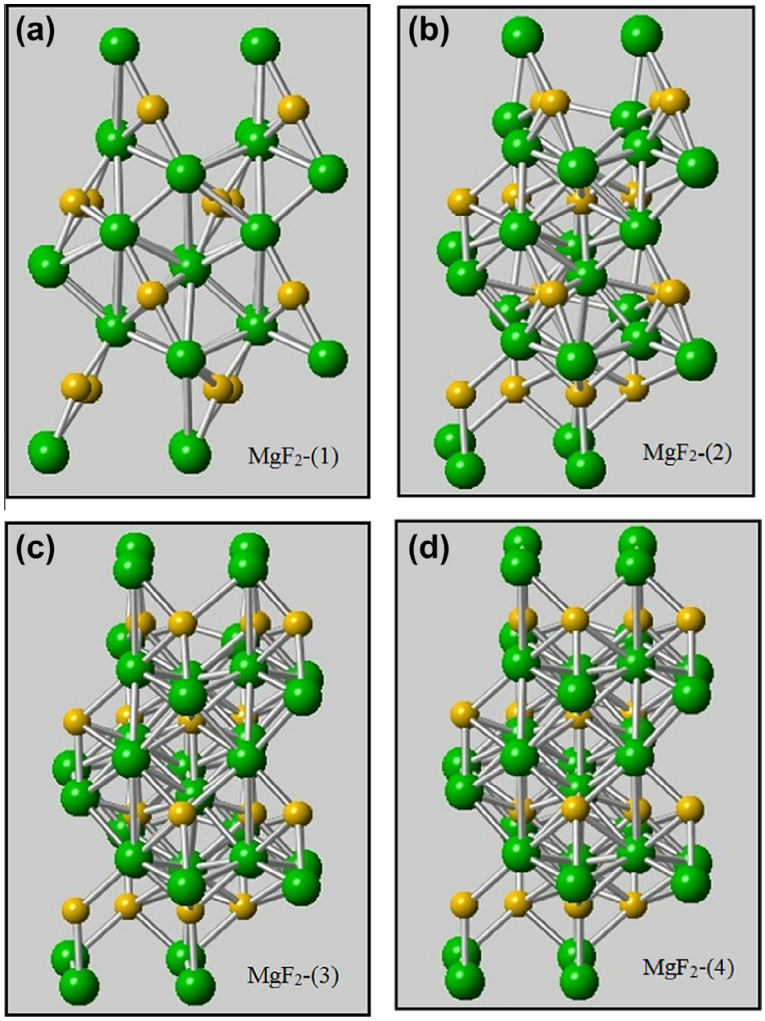

Fig. 3. At 90 GPa, evolution of the α-$PbCl_2$-type structure at minimization steps such as (a) MgF_2-(1) at Step 412, (b) MgF_2-(2) at Step 517, (c) MgF_2-(3) at Step 553 and (d) MgF_2-(4) at Step 580. All structures are viewed along *z*-direction.

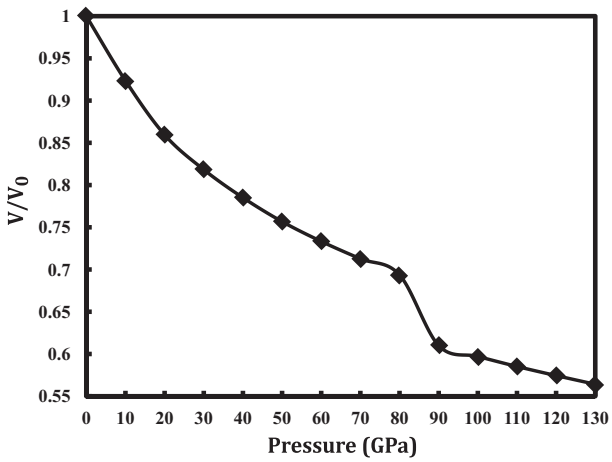

Fig. 4. Pressure–volume curve of MgF_2 from the constant-pressure ab initio simulations.

the computed enthalpy curves as a function of pressure. We can conclude from these curves that the first phase transformation from the rutile structure to the $CaCl_2$-type structure with space group *Pnnm* occurs at about 9 GPa, comparable with the experimental result of 9.1 GPa (Ref. [9]) and the second phase transformation from the $CaCl_2$-type structure to the α-$PbCl_2$-type structure with space group *Pnma* occurs at about 35 GPa, which agree with the theoretical result of 35 GPa Ref. [10]. These phases were obtained also at 9 GPa and 40 GPa by Zhang et al. [11]. Thus, we expect to observe these phase transitions in experiments about these pressures. The results of this study are comparable with experimental and theoretical values.

As seen in the Table 2, the used simulation technique gives comparable results with experiments and theoretical calculations

Table 1
The equilibrium lattice parameters and the atomic fractional coordinates of the rutile-type, $CaCl_2$-type and α-$PbCl_2$-type structures.

Structure	*a* (Å)	*b* (Å)	*c* (Å)	*x*	*y*	*z*
Rutile-type	4.6038	4.6038	3.0734	Mg : 0.5000	0.5000	0.5000
				F : 0.8043	0.8043	0.5000
				F : 0.1957	0.1957	0.5000
$CaCl_2$-type	4.2247	4.4874	2.9533	Mg : 0.5000	0.5000	0.5000
				F : 0.7615	0.7615	0.5000
				F : 0.2385	0.8424	0.5000
α-$PbCl_2$-type	4.8011	2.9166	5.6763	Mg : 0.2501	0.2500	0.8853
				F : 0.8535	0.2500	0.9279
				F : 0.4778	0.2500	0.1680

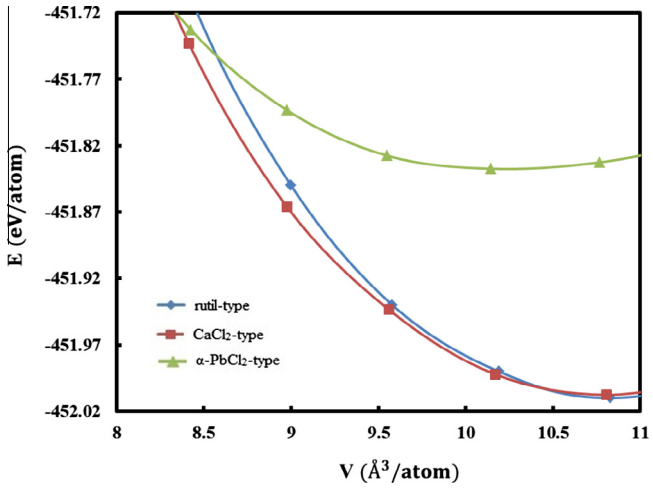

Fig. 5. The energy curves of MgF_2 structures as function of volume (rutil-type structure marked with "—◆—", $CaCl_2$-type structure with "—■—" and α-$PbCl_2$-type structure with "—▲—") (For interpretation of the references to colour in this figure legend, the reader is referred to the web version of this article.).

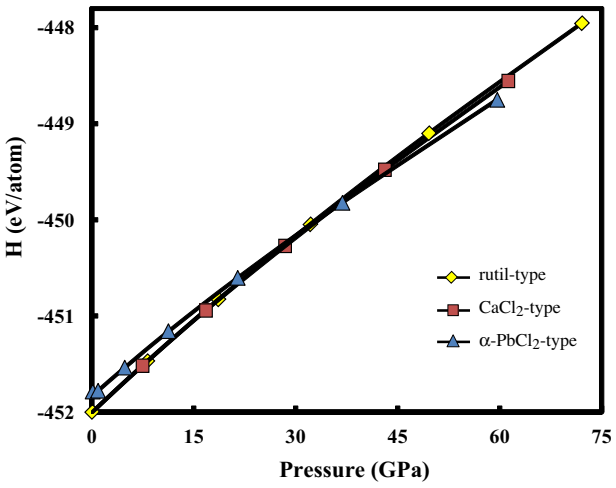

Fig. 6. The enthalpy curves of MgF_2 (rutile-type structure marked with "—◆—", $CaCl_2$-type structure with "—■—" and α-$PbCl_2$-type structure with "—▲—") (For interpretation of the references to colour in this figure legend, the reader is referred to the web version of this article.).

Table 2
Transition pressures, equilibrium lattice parameters, equilibrium volume rates, the bulk modules and their pressure derivatives of MgF_2 phases.

Structure	Pressure (GPa)	a (Å)	b (Å)	c (Å)	V/V_0	B_0 (GPa)	B_0'	Ref.
Rutil-type	0	4.6038	4.6038	3.0734	1	117	4.13	This study
		4.6249	4.6249	3.0520	1[a]	98	3.70	[9]
		4.6213	4.6213	3.0519	1[a]	101	4.20	[9] (Expt.)
		4.6280	4.6280	3.0450				[9] (Expt.)
		4.5720	4.5720	3.0170		101		[10]
		4.6250	4.6250	3.0520		101		[10] (Expt.)
		4.6912	4.6912	3.0960		97	3.70	[11]
		4.6080	4.6080	3.0070				[17]
						101.7	3.85	[34] (Expt.)
		4.6460	4.6460	3.1070				[35]
$CaCl_2$-type	9	4.2247	4.4874	2.9533	0.8595	109.3	3.65	This Study
	12.3				1.0060[a]	82	3.70	[9]
	9.1							[9] (Expt.)
	10	4.4190	4.6400	2.8280		134		[10]
		4.5360	5.6460	3.5690				[17]
		4.5920	4.9380	2.9590				[35]
α-$PbCl_2$-type	35	4.8011	2.9166	5.6763	0.6101	66.72	5.32	This Study
					0.8130[a]	158	3.50	[9]
	35				0.7600[a]	163	7	[9] (Expt.)
		5.1040	5.7160	3.0450		259		[10]
						163		[10] (Expt.)

[a] Equation of state data.

[9–11,17,34,35]. Among the results, equilibrium lattice parameters and equilibrium volume rates of rutile-type structure are the best compatible with the literature. Figs. 7 and 8 illustrate the structures with polyhedral views obtained in that study. The coordination number for the Mg in each phase is 6, 6, 9, 6, 9, 9 and 9 for rutile-type, $CaCl_2$-type, α-$PbCl_2$-type, MgF_2-(1), MgF_2-(2), MgF_2-(3) and MgF_2-(4), respectively.

4. Conclusions

We have studied the high-pressure behavior of MgF_2 via an ab initio constant pressure technique. Two high-pressure phases and three intermediate phases were predicted in the simulations. Although these high-pressure phases are comparable to the findings of previous studies, the intermediate phases obtained in our study have not been observed in any other earlier studies. The

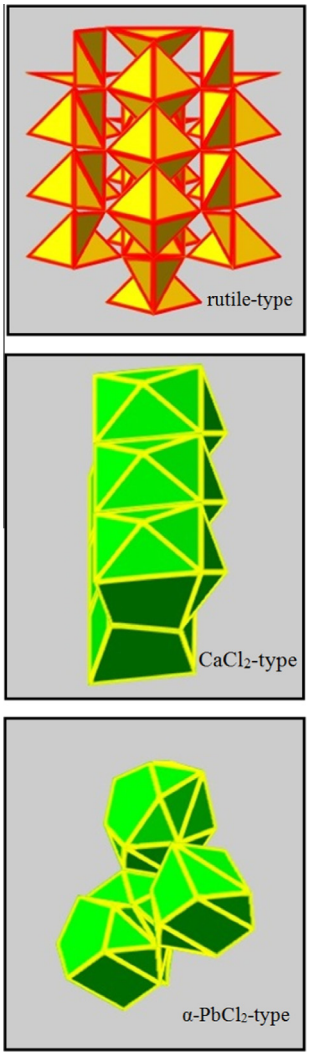

Fig. 7. Crystal structures with polyhedral views of MgF_2: rutile-type structure at zero pressure (as illustrated in the first panel), $CaCl_2$-type structure at 20 GPa (in the second panel) and α-$PbCl_2$-type structure at 90 GPa (in the third panel). All structures are viewed along [1 1 1] directions.

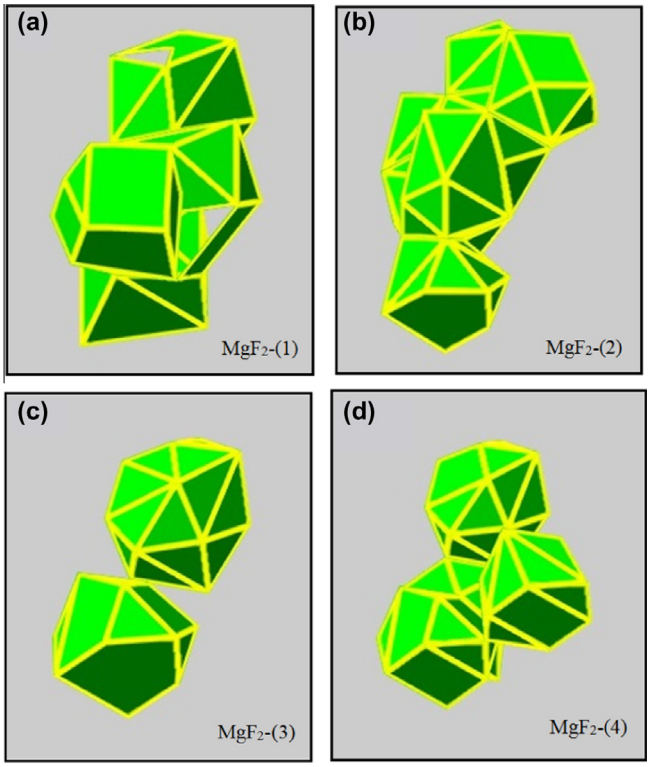

Fig. 8. At 90 GPa, crystal structures with polyhedral views of the α-$PbCl_2$-type structure at minimization steps such as (a) MgF_2-(1) at Step 412, (b) MgF_2-(2) at Step 517, (c) MgF_2-(3) at Step 553 and (d) MgF_2-(4) at Step 580. All structures are viewed along [1 1 1] directions.

phase transformation from the $CaCl_2$-type structure to the α-$PbCl_2$-type structure is based on these three intermediate phases with space groups $P2_1/m$, $P2_1$ and $P2_12_12_1$. Our findings allow different viewpoints on the transformation mechanism of the $CaCl_2$-type structure to the α-$PbCl_2$-type structure phase change. Reliable dynamical simulations are desirable due to the restrictions of experimental information at the atomistic level. Such simulations may identify the microscopic nature of transformation mechanisms of phases for each applied pressure.

Acknowledgements

This work was supported by the Ahi Evran University under Scientific Research Project (BAP) No: FBA-10-14. The authors are grateful to the referees for many suggestions which led to an improved version of this paper.

References

[1] R.S. Katıyar, J. Phys. C: Solid State Phys. 3 (1970) 1693–1702.
[2] W.H. Baur, Acta Cryst. B 32 (1976) 2200–2204.
[3] M. Catti, A. Pavese, R. Dovesi, C. Roetti, M. Causa, Phys. Rev. B 44 (1991) 3509–3517.
[4] Y.A. Nga, C.K. Ong, J. Chem. Phys. 98 (1993) 3240–3245.
[5] N.L. Allan, R.I. Hines, M.D. Towler, W.C. Mackrodt, J. Chem. Phys. 100 (1994) 4710–4711.
[6] K. Nishidate, M. Baba, T. Sato, K. Nishikawa, Phys. Rev. B 52 (1995) 3170–3176.
[7] G.D. Barrera, M.B. Taylor, N.L. Allan, T.H.K. Barron, L.N. Kantorovich, W.C. Mackrodt, J. Chem. Phys. 107 (1997) 4337–4344.
[8] E. Francisco, J.M. Recio, M.A. Blanco, A. Martın Pendás, A. Costales, J. Phys. Chem. A 102 (1998) 1595–1601.
[9] J. Haines, J.M. Leger, F. Gorelli, D.D. Klug, J.S. Tse, Z.Q. Li, Phys. Rev. B 64 (2001) 134110.
[10] V. Kanchana, G. Vaitheeswaran, M. Rajagopalan, J. Alloys Comp. 352 (2003) 60–65.
[11] L. Zhang, Y. Wang, T. Cui, Y. Ma, G. Zou, Solid State Commun. 145 (2008) 283–287.
[12] K. Kusuba, T. Kikegawa, Solid State Commun. 148 (2008) 440–443.
[13] K.R. Babu, Ch.B. Lingam, S. Auluck, S.P. Tewari, G. Vaitheeswaran, J. Solid State Chem. 184 (2011) 343–350.
[14] X.W. Sun, T. Song, Z.J. Liu, C.R. Zhang, J.H. Tian, P. Guo, Solid State Commun. 151 (2011) 1507–1510.
[15] J.H. Tian, T. Song, X.W. Sun, Z.J. Liu, W.L. Quan, P. Guo, Physica B 407 (2012) 551–554.
[16] M.A.C. Wevers, J.C. Schön, M. Jansen, J. Solid State Chem. 136 (1998) 233–246.
[17] M.A.C. Wevers, J.C. Schön, M. Jansen, J. Phys.: Condens. Matter 11 (1999) 6487–6499.
[18] X. Mu, S. Neelamraju, W. Sigle, C.T. Koch, N. Toto, J.C. Schön, A. Bach, D. Fischer, M. Jansen, P.A. van Aken, J. Appl. Crystallogr. 46 (2013) 1105–1116.
[19] K.H. Hoffmann, J.C. Schön, Eur. Phys. J. B 86 (2013) 220–229.
[20] P. Ordejon, E. Artacho, J.M. Soler, Phys. Rev. B 53 (R10) (1996) 441–444.
[21] J.P. Perdew, K. Burke, M. Ernzerhof, Phys. Rev. Lett. 77 (1996) 3865–3868.
[22] E. Artacho, D. Sanchez-Portal, P. Ordejon, A. Garcia, J.M. Soler, Phys. Status Solidi (b) 215 (1999) 809–817.
[23] N. Troullier, J.L. Martins, Phys. Rev. B 43 (1991) 1993–2006.
[24] H.J. Monkhorst, J.D. Pack, Phys. Rev. B 13 (1976) 5188–5192.
[25] M. Parrinello, A. Rahman, Phys. Rev. Lett. 45 (1980) 1196–1199.
[26] A. Hannemann, R. Hundt, J.C. Schön, M. Jansen, J. Appl. Crystallogr. 31 (1998) 922–928.
[27] R. Hundt, J.C. Schön, A. Hannemann, M. Jansen, J. Appl. Crystallogr. 32 (1999) 413–416.
[28] S. Lopez-Moreno, A.H. Romero, J. Mejıia-Lopez, A. Munoz, I.V. Roshchin, Phys. Rev. B 85 (2012) 134110.
[29] F. Birch, Phys. Rev. 71 (1947) 809–824.
[30] F.D. Murnaghan, Proc. Natl. Acad. Sci. USA 30 (1944) 244–247.
[31] R.A. Evarestov, E. Blokhin, D. Gryaznov, E.A. Kotomin, J. Maier, Phys. Rev. B 83 (2011) 134108.
[32] X. Luo, W. Zhou, S.V. Ushakov, A. Navrotsky, A.A. Demkov, Phys. Rev. B 80 (2009) 134119.
[33] M. Durandurdu, J. Phys.: Condens. Matter 20 (2008) 325232–325237.
[34] J.K. Vassiliou, J. Appl. Phys. 57 (1985) 4543–4547.
[35] A. Neelamraju, J. Bach, C. Schön, D. Fischer, M. Jansen, J. Chem. Phys. 137 (2012) 194319.